Atmospheric Environment 61 (2012) 361–370

Contents lists available at SciVerse ScienceDirect

Atmospheric Environment

journal homepage: www.elsevier.com/locate/atmosenv

A semi-empirical, receptor-oriented Lagrangian model for simulating fine particulate carbon at rural sites

B.A. Schichtel [a,*], M.A. Rodriguez [b], M.G. Barna [a], K.A. Gebhart [a], M.L. Pitchford [c], W.C. Malm [b]

[a] National Park Service, CIRA/CSU, 1375 Campus Delivery, Fort Collins, CO 80523, USA
[b] Cooperative Institute for Research in the Atmosphere, Colorado State University, Fort Collins, CO 80523, USA
[c] Division of Atmospheric Sciences, Desert Research Institute, Reno, NV 89512, USA

HIGHLIGHTS

- We present a new semi-empirical Lagrangian particle dispersion model.
- The model is used to apportion $PM_{2.5}$ carbon at rural locations to major source types.
- The results are evaluated against measured data and compared to CMAQ model results.
- The model is best used in the analysis of measured carbonaceous aerosols.

ARTICLE INFO

Article history:
Received 24 October 2011
Received in revised form
9 April 2012
Accepted 6 July 2012

Keywords:
Lagrangian particle dispersion model
Carbonaceous aerosols
Source apportionment
Biomass burning

ABSTRACT

Total fine particulate carbon (TC) is an important contributor to fine particulate matter and is measured in routine national monitoring programs. TC contributes to adverse health effects, regional haze, and climate effects. To resolve these adverse effects, there is a need for tools capable of routine and climatological assessments and exploration of the sources contributing to the measured TC. To address this need, a receptor-oriented, Lagrangian particle dispersion model was developed to simulate TC in rural areas, using readily available meteorological and emission inputs. This model was based on the CAPITA (Center for Air Pollution Impact and Trend Analysis) Monte Carlo model (CMC) and simulated the contributions from eight source categories, including biomass burning and secondary organic carbon (SOC) from vegetation. TC removal and formation mechanisms are simulated using a simplified parameterization of atmospheric processes based on pseudo-first-order rate equations. The rate coefficients are empirical functions of meteorological parameters derived from measured, modeled, and literature data. These functions were optimized such that the simulated TC concentrations reproduce the average spatial and seasonal patterns in measured 2008 U.S. TC concentrations, as well as measured SOC fractions at two eastern U.S. sites. The optimized model was used to simulate 2006–2008 rural TC that was evaluated against measured TC. In addition, the model output was compared to TC from a 2006 Eulerian Community Multiscale Air Quality (CMAQ) simulation. It is shown that the CMC model has similar performance metrics as the CMAQ model.

Published by Elsevier Ltd.

1. Introduction

Carbonaceous aerosols arise from a wide variety of sources, including combustion of fossil fuels, meat cooking, deep frying, and biomass burning (Bond et al., 2004). Secondary organic carbon (SOC) produced from biogenic and combustion volatile organic compounds (VOCs) also contribute to organic aerosols. The diverse carbon sources and atmospheric processing result in a complex mixture of compounds that significantly contribute to fine particulate matter (PM) < 2.5 μm ($PM_{2.5}$) (Hand et al., 2012). High $PM_{2.5}$ carbon concentrations can lead to adverse health effects, their efficient scattering and absorption of visible and infrared radiation make them a key factor in the balance of solar radiation, and they contribute to haze in protected national parks and wilderness areas, i.e., class I areas.

The Interagency Monitoring of Protected Visual Environments (IMPROVE) and Chemical Speciation Network (CSN) routine monitoring networks collect 24-h, integrated $PM_{2.5}$ samples that are analyzed for chemical composition, including organic (OC) and elemental (EC) carbon. The IMPROVE monitoring program is used

* Corresponding author. Tel.: +1 970 491 8581; fax: +1 970 491 8598.
E-mail address: Schichtel@cira.colostate.edu (B.A. Schichtel).

1352-2310/$ – see front matter Published by Elsevier Ltd.
http://dx.doi.org/10.1016/j.atmosenv.2012.07.017

to track long-term trends in visibility and haze in protected visual environments, consistent with the needs of the Regional Haze Rule. Data are also used to identify chemical species and emission sources responsible for the haze. The objectives of the CSN are to track progress of emission control programs, develop emission control strategies, and characterize spatial and temporal trends in speciated $PM_{2.5}$.

To achieve the goals of these monitoring programs, there is a need for tools capable of routine and climatological assessments and exploration of the causes of the measured carbonaceous and other aerosol concentrations. Available tools range from simple back trajectory models to sophisticated Eulerian chemical transport models (CTM). Back trajectory/dispersion models are efficient models capable of simulating multiple years of airmass transport to one or more receptors, using readily available meteorological data. Trajectory analysis methods generally do not incorporate emissions or simulate atmospheric removal/formation processes and use some variation of the residence time analysis method (Ashbaugh, 1983). They qualitatively identify transport pathways and broad regions where sources are likely to contribute to the measured receptor concentrations. Due to their simplicity and value, trajectory analysis methods have seen widespread use in a variety of analyses (e.g., Stohl, 1998).

Eulerian CTMs are capable of quantitative assessments of the contributions of source regions and types contributing to the receptor concentrations. However, CTMs are generally resource intensive, requiring a variety of data inputs and computer and personnel resources. Consequently, source apportionment is typically performed in short-term studies by dedicated modeling groups, limiting the applicability of these important tools.

In this work we strove to develop a quantitative data assessment tool more akin to trajectory analyses than Eulerian CTMs that is capable of apportioning carbonaceous aerosol measured at remote-area monitoring sites to contributing source types, including biomass burning, mobile, and vegetation. A primary goal was that the model be readily applicable to short- and long-term data analysis studies, requiring the same meteorological inputs as used in trajectory models, with the only additional data input being emission fields.

To accomplish this, the receptor-oriented (backward time) Lagrangian particle dispersion model (LPDM) (Uliasz and Pielke, 1992) approach was used. Receptor-oriented LPDMs model the receptor concentration as an ensemble of particles that are dispersed back in time. These models readily lend themselves to efficient source apportionment analyses, since they directly simulate the source–receptor relationship by maintaining a separation between sources. In addition, only sources upwind of the monitoring sites are simulated, making this approach advantageous for investigating monitoring data where there are a limited number of receptor sites (Seibert and Frank, 2004). To simulate atmospheric physical and chemical removal and formation processes, a simplified parameterization based on pseudo-first-order rate equations was developed. The rate coefficients are functions of meteorological parameters and are optimized through a tuning process to fit measured data. Others have used and proposed LPDMs for quantitative simulation and assessments of receptor concentrations (e.g., Seibert and Frank, 2004); however, all receptor LPDMs of which we are aware have employed linear loss and gain mechanisms and have not simulated the formation of secondary pollutants.

The model was developed and optimized using the IMPROVE total fine particulate carbon (TC), i.e., the sum of the measured OC and EC, at rural monitoring sites during 2008, as well as measured SOC fractions at two eastern U.S. sites. It was then used to simulate the 2006–2007 IMPROVE TC concentrations. Following is a description of the model formulation, the optimization process, and the evaluation of simulated concentrations from 2006 – 2008 IMPROVE data. In addition, in the Supplementary material the 2006 model simulation is compared to the results from the Community Multiscale Air Quality Modeling System (CMAQ) Eulerian CTM. A following paper will examine the source contribution results from the 3-year model simulation.

2. Receptor-oriented particulate carbon chemical transport modeling

Conceptually, the receptor-oriented chemical LPDM works by assuming that the concentration or mixing ratio of a trace species can be represented by the average from an ensemble of particles or air parcels at the receptor location and time. These particles are first dispersed for a fixed period back in time, with each particle following a unique back trajectory due to random atmospheric turbulence. At the end of the particles' trajectories, they are given an initial concentration and then transported forward in time, following their trajectory pathways back to the receptor. During this forward transport, mass balance is maintained at the particle level by modifying its initial concentration by emissions accumulated along the trajectory pathway and physical/chemical processes, including deposition and chemical transformations.

For the simulation of fine particulate carbon, this method requires four components: first, a backward LPDM and meteorological input data to simulate the history of the receptor airmass; second, an emission inventory accounting for emissions from various source types of particulate carbon and VOCs; third, a model formulation relating the emissions from sources traversed by the trajectories to the receptor concentration and the changes in these emissions due to atmospheric physical and chemical processes during transport. In this application, the last component entails parameterization of physical and chemical processes and their optimization to fit measured data.

2.1. CAPITA Monte Carlo LPDM

The calculation of the receptor airmass histories for the simulation of particulate carbon at IMPROVE monitoring sites was conducted using the CAPITA (Center for Air Pollution Impact and Trend Analysis) Monte Carlo (CMC) LPDM. The formulation of the CMC LPDM model and its use for forward and backward dispersion simulations has been described elsewhere (Schichtel and Husar, 1997; Schichtel et al., 2005a).

The CMC model is capable of simulating forward and backward dispersion, using different meteorological fields and from one to thousands of particle trajectories. In this work, the National Centers for Environmental Prediction (NCEP) Eta Data Assimilation System (EDAS) (Black, 1994) meteorological data were used. The EDAS meteorological fields are archived at the National Oceanic and Atmospheric Administration (NOAA) Air Resource Laboratory (ARL) using a 40-km grid and 26 pressure surfaces every 3 h.

Many of the IMPROVE monitors are located in complex terrain. The Lagrangian model and coarse meteorological data are not suited for simulating potentially important mesoscale features, including channeling by terrain and convective precipitation. However, they are suitable for simulating regional-scale features, and it is assumed that it is regional-scale emissions and meteorology that are causing most of the variance in the measured concentrations. As will be shown, the model performance decreases in urban areas and when local fires are present. This decreased performance may partly be due to the difficulty of simulating the transport at the smaller scales.

2.2. Particulate and VOC emission fields

A detailed 2002 emission inventory for input into Eulerian chemical transport models using the CBM-IV chemical mechanism was developed for the Western Regional Air Partnership (WRAP) and used to simulate the impact of PM and haze on national parks and wilderness areas in support of Regional Haze Rule State Implementation Plans (Brewer and Moore, 2009). This emission inventory had hourly emission rates from 22 area, point, mobile, and biogenic source categories for 21 different species, including OC and EC and eight groups of reactive VOC compounds. The area sources were on a 36-km modeling domain covering most of North America and a nested 12-km grid covering most of the western United States.

The 36-km WRAP emissions were used for input into the CMC model. The emissions from the point sources were summed with the area source in the grid cell into which each point source fell. In addition, the hourly emission rates were averaged up to 24-h values, and the 22 source categories were grouped into six categories as defined in Table 1. The eight VOC emission categories were aggregated into three categories consisting of a high carbon number and SOA yield group (Zhang et al., 2007), a low carbon number and SOA yield group, and isoprene (Table 2). Isoprene was separated from the other compounds because it has low SOA yields, but its high emissions result in significant contributions to SOA (Kleindienst et al., 2007; Carlton et al., 2009). The units of the VOC emission rates were converted to kg C m^{-2} day^{-1} using the carbon numbers in Table 2. These aggregated 2002 emissions were used for simulating particulate carbon in all modeled years.

Biomass burning is a significant source of TC, and the emission locations, release times, and rates have large variations from one year to another. The WRAP biomass burning emissions were replaced by the National Center for Atmospheric Research (NCAR) regional fire emissions model version 2.0 (Wiedinmyer et al., 2006). This is a North American inventory that estimates the daily fire emissions of OC, EC, total VOC, and other species from individual fires. The location and timing of the fires were determined by observations from the Moderate Resolution Imaging Spectroradiometer (MODIS) instruments aboard the Terra and Aqua satellites, and each fire encompassed an area burned up to 1 km^2.

The individual fires in the emission inventory were gridded to the same 36-km grid used for the WRAP inventory by aggregating all fires that fell into the same grid cell. There is evidence that fire emission inventories overestimate the primary carbon emissions and underestimate the semivolatile OC and subsequent formation of SOC (Hennigan et al., 2011). This was also seen in initial model simulations in which receptors near fires typically overestimated the TC. To account for this, the primary emissions were evenly distributed over 8 h from the release of the fire's emissions. The tracking of the primary TC and formation of this pseudo-SOC was done along each particle's trajectory. Based upon land-use data in the NCAR fire emission inventory, the fires were classified as either agricultural or other fires.

Table 1
Emission categories used in the CMC model.

Source category	Emission inventory	Description
Area	WRAP	Stationary area sources, e.g., residential heating and architectural coatings
Point	WRAP	Point sources, e.g., electrical generating units and oil refineries
Mobile	WRAP	On- and off-road mobile sources
Biogenic	WRAP	Vegetation gaseous emissions
Oil and gas	WRAP	Oil and gas in the western United States
Other	WRAP	Off shore sources, e.g., shipping, and road, fugitive, and windblown dust
Agricultural fires	NCAR	Agricultural fires
Other fires	NCAR	Wild and prescribed fires

Table 2
VOC categories from the CBM-IV chemical mechanism and their corresponding carbon numbers, combined into high and low reactive VOC categories.

	VOC category	Carbon #
High reactive VOC	Toluene and other monoalkyl aromatics	7
	Xylene and other polyalkyl aromatics	8
	Terpenes	10
Low reactive VOC	Formaldehyde	1
	Higher aldehyde	2
	Ethene	2
	Paraffin carbon bond (C–C)	1
	Olefin carbon bond (C=C)	2
Isoprene	Isoprene	5

2.3. Chemical transport LPDM formulation

There are various formulations of the receptor-oriented LPDM. In this work we follow that set forth by Seibert and Frank (2004), which was based on mixing ratios and incorporated first-order rate processes. In the Lagrangian framework, they showed that the mixing ratio χ at time t and location r^* for a species affected by first-order processes that can vary in space and time for a single particle's trajectory is

$$\chi\left(r^*, t\right) = \chi_o p(0) + \int_{t-\tau}^{t} \frac{\dot{q}[\mathbf{r}(t'), t']}{\rho[\mathbf{r}(t'), t']} p(t') \mathrm{d}t' \quad (1)$$

where

τ is the length of the particle back trajectory in time, units [s]
χ_o is the particle's initial mixing ratio at time $t - \tau$.
$\dot{q}$ is the source emission rate, units [g m^{-3} s^{-1}]
ρ is air density, units [g m^{-3}]
$p(t')$ is the transmission function, i.e., the loss or gain in mass due to first-order rate processes during transport from the source to the receptor along the trajectory during time period $t - t'$.

Space and time can be discretized such that space is gridded with index i; time at the receptor has index j; and time along each trajectory has N equal time steps with index n. It can then be shown that Eq. (1) becomes

$$\chi_j \approx \chi_o p(0) + \sum_i \sum_{n=j-N}^{j} \left(\frac{\dot{q}_{in}}{\rho_{in}} \Delta t'_{in} p_{in} \right) \quad (2)$$

where

$\Delta t'_{in}$ is the residence time of the particle in grid i during the time step n

p_{in} is the loss or gain in mass from time of the emissions n in grid cell i to impacting the receptor at time j.

The average mixing ratio at the receptor over a time period J and the ensemble of particles M at each time step j is then

$$\overline{\chi} = \frac{1}{J^* M} \sum_{j=j'}^{j'+J} \sum_{m=0}^{M} \chi_{jm} \quad (3)$$

The average source contribution can be calculated by

$$G_{ji} = \frac{1}{J^{*}M}\sum_{j=j'}^{j'+J}\sum_{m=0}^{M}\sum_{n=j-N}^{j}\left(\frac{\dot{q}_{in}}{\rho_{in}}\Delta t'_{in}p_{in}\right) \quad (4)$$

In Eq. (4), i represents a source region; however, in application it could also be an individual source or source type.

2.3.1. Particulate carbon physical/chemistry model

The backward LPDM formulated in Eqs. (2) and (3) can accommodate any first-order process $P(t)$ that describes the change in concentrations due to physical/chemical processes over a given time period. In this work we are interested in simulating TC. TC is a mixture of primary OC and EC and SOC compounds formed by the oxidation and condensation of VOCs. The particulate and gaseous species can be removed from the atmosphere by dry and wet deposition. These processes can be modeled using the coupled sets of rate equations:

$$\frac{\mathrm{d}(\mathrm{VOC}_i)}{\mathrm{d}t} = -\left(k_i^t + k_{g_i}^{\mathrm{d}} + k_{g_i}^{\mathrm{w}}\right)\mathrm{VOC}_i \quad (5)$$

$$\frac{\mathrm{d}(\mathrm{TC})}{\mathrm{d}t} = \left(\sum_i k_i^t(\mathrm{VOC}_i)\right) - \left(k_{\mathrm{p}}^{\mathrm{d}} + k_{\mathrm{p}}^{\mathrm{w}}\right)\mathrm{TC} \quad (6)$$

where

TC is the particulate carbon mixing ratio
VOC_i is an individual or class of VOC mixing ratio
k_i^t, $k_{g_i}^{\mathrm{d}}$, and $k_{g_i}^{\mathrm{w}}$ are VOC gas to particulate carbon transformation, dry deposition, and wet deposition rate coefficients, respectively
$k_{\mathrm{p}}^{\mathrm{d}}$ and $k_{\mathrm{p}}^{\mathrm{w}}$ are particulate carbon dry and wet deposition rate coefficients, respectively.

Although the rate equations are linear, the species-specific transformation rate coefficients and dry and wet deposition rates can be nonlinear functions dependent upon the chemical, meteorological, and geological environment of the species. Physical formulations can be developed to model these processes. However, these formulations typically require extensive information and data that are often unavailable or difficult to obtain, requiring a number of assumptions that can lead to large uncertainties. An alternative approach is to develop empirical relationships between the coefficients and readily available meteorological, chemical, and geophysical variables where the relationships are optimized so that the simulated concentrations are a best fit to measured values (Schichtel and Husar, 1997). The empirical approach was used, since the intent of this work was to develop a model that captures important spatial and temporal variability but has modest data requirements and can be routinely operated.

2.4. Empirical rate coefficient equations

Dry deposition is a flux of material to the surface and is often modeled as the product of a deposition velocity v_{d} and the species concentration. The dry deposition coefficient, k^{d}, for a given species is then

$$k^{\mathrm{d}} = \frac{v_{\mathrm{d}}}{\mathrm{H}}, \quad (7)$$

where

H is the layer near the surface where dry deposition occurs.

The dry deposition velocity of particulates ($v_{\mathrm{d}}^{\mathrm{p}}$) and gases ($v_{\mathrm{d}}^{\mathrm{g}}$) are determined by atmospheric mixing, which delivers material to the surface, and by the absorptive properties of the surface. Both of these processes vary spatially, diurnally, and seasonally, influenced by the solar insulation. Consequently, relationships between v_{d} and solar insulation were sought.

To explore this relationship, $v_{\mathrm{d}}^{\mathrm{p}}$ from the Clean Air Status and Trends Network (CASTNET) dry deposition monitoring program and VOC $v_{\mathrm{d}}^{\mathrm{g}}$ from a Comprehensive Air quality Model with extensions (CAMx) simulation over most of North America were compared to the surface downward shortwave radiation flux (SR) [kW m^{-2}] from the EDAS meteorological fields. In the CASTNET monitoring program, hourly $v_{\mathrm{d}}^{\mathrm{p}}$ are calculated for each monitoring site, using the Multilayer Deposition Velocity Model (MLM) (Meyers et al., 1998). The CAMx data were from a 2009 simulation similar to Rodriguez et al. (2011).

Fig. 1 compares the average diurnal cycle of the $v_{\mathrm{d}}^{\mathrm{p}}$ against SR for the months of January, April, July, and October. The CASTNET $v_{\mathrm{d}}^{\mathrm{p}}$ diurnal cycle was calculated by averaging $v_{\mathrm{d}}^{\mathrm{p}}$ over all CASTNET sites from 2000 through 2005 for each hour of the day. As shown, these average $v_{\mathrm{d}}^{\mathrm{p}}$ and SR values are highly correlated, with $r^2 = 0.98$, and all months have a similar linear relationship.

Fig. 2 compares the average diurnal cycle of a VOC-concentration-weighted average $v_{\mathrm{d}}^{\mathrm{g}}$ to SR. The hourly composite VOC $v_{\mathrm{d}}^{\mathrm{g}}$ were calculated from the CAMx model results at each IMPROVE site. The average $v_{\mathrm{d}}^{\mathrm{g}}$ for most VOCs varied between 0.03 and 0.4 cm s^{-1}, though some short-lived-reaction products had average $v_{\mathrm{d}}^{\mathrm{g}} > 2$ cm s^{-1}. As shown in Fig. 2, the aggregated $v_{\mathrm{d}}^{\mathrm{g}}$ diurnal cycle is highly correlated with SR and has a quadratic relationship that varies by season, with higher $v_{\mathrm{d}}^{\mathrm{g}}$ during July than January. The $v_{\mathrm{d}}^{\mathrm{g}}$ values during April and October are similar and are between July and January.

There are physical explanations for the v_{d} relationships with SR. In the MLM, $v_{\mathrm{d}}^{\mathrm{p}}$ is highly dependent upon the aerodynamic layer resistances, and this resistance is dependent on atmospheric turbulence (Vong et al., 2010). It appears that SR is a good surrogate for this turbulence and on average $v_{\mathrm{d}}^{\mathrm{p}}$ is approximately linearly dependent on SR. Dry deposition of gases is also dependent on the canopy resistance, and as modeled in CAMx, the canopy resistance is inversely dependent on SR^2 (ENVIRON, 2010).

Based on these results, $v_{\mathrm{d}}^{\mathrm{p}}$ and $v_{\mathrm{d}}^{\mathrm{g}}$ were parameterized as linear and quadratic functions of SR, respectively. These functions account for the average diurnal and seasonal variation in v_{d} but do not account for the day to day variation in other important

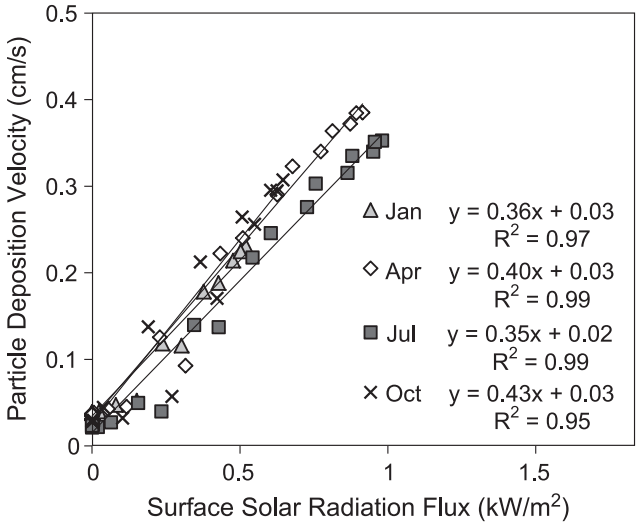

Fig. 1. Scatter plots showing the relationship between the average diurnal cycle in the particle dry deposition velocity from the CASTNET program and solar radiation for January, April, July, and October.

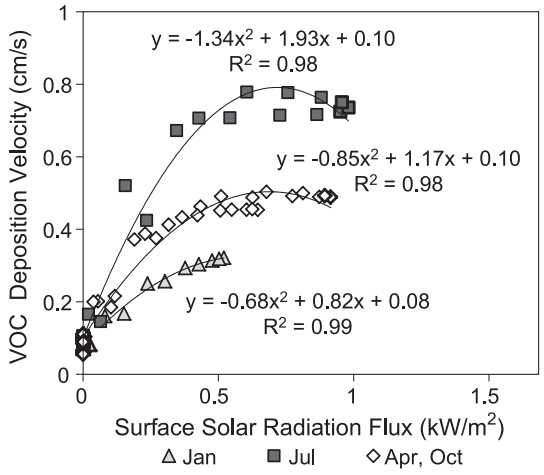

Fig. 2. Scatter plots showing the relationship between the average diurnal cycle in the effective VOC dry deposition velocity derived from CAMx and solar radiation for January, April, July, and October.

meteorological parameters and changing land surface types. These influences are significant, and the coefficients of variation for a given season and hour of the day for both v_d^p and v_d^g were on the order of one.

Wet deposition can be parameterized by introducing a dimensionless washout ratio W, which is the ratio of the concentration of the species in the precipitation to its concentration in the air. The wet removal rate or scavenging coefficient for a given species is then

$$k^w = \frac{W}{H_w} P, \tag{8}$$

where

H_w is a washout depth (m) and P is the precipitation rate (m s^{-1}) (Barrie, 1981; Andronache, 2004).

TC washout ratios vary depending on precipitation types and particulate properties, including size and hygroscopicity, and can vary by several orders of magnitude, though typical values range from 10^5 to 10^6 (Bidleman, 1988). It is commonly assumed that a slightly soluble trace species in the atmosphere is in equilibrium with a falling raindrop. Under this condition of equilibrium gas scavenging, as discussed by Hart et al. (1993), the washout ratio can be estimated as

$$W_g = \frac{RT}{k_H}, \tag{9}$$

where

R (m^3 atm (K mol)$^{-1}$) is the universal gas constant

T (K) is the temperature
k_H (M atm^{-1}) is the species effective Henry Law constant.

k_H for different VOC species varies over several orders of magnitude. Using the VOC concentrations from the 2009 CAMx model simulation at each IMPROVE site and the k_H for each VOC species at 298 K (ENVIRON, 2010), a concentration-weighted composite VOC k_H for the January, April, July, and October months was calculated that varied from 10^3 to 2×10^3 M atm^{-1}. These k_H correspond to W_g from 2.3×10^4 to 5.2×10^4.

These TC and VOC washout ratios are large and under moderate to heavy precipitation will efficiently remove most carbonaceous species from the atmosphere. Therefore, only constant average washout ratios were used in the model.

SOA formation in the atmosphere is dependent on a number of factors, and not all relevant processes are well understood, leading to broad ranges and high uncertainties in modeled formation rates and making this an active area of research (Carlton et al., 2009; Hallquist et al., 2009; Hennigan et al., 2011). Most SOC formation is driven by photochemical processes and is dependent on SR. Non-photochemically driven reactions may also be important; for example, Ng et al. (2008) showed that the SOC formation could occur from nighttime reactions of isoprene with nitrate radicals. Evidence also exists for significant aqueous-phase SOA formation (Hallquist et al., 2009).

Given these complications and unknowns, the transformation rate for the high-yield VOCs was made a linear function of SR. The transformation rate for the low-yield VOCs and isoprene was set to a constant fraction of the high-yield VOCs. In order to account for aqueous-phase SOA, these transformation rates were increased by 50% during precipitation periods.

2.5. Implementation and optimization of the CMC model for TC simulation

The CMC model was used to simulate the receptor airmass dispersion at 162 IMPROVE monitoring sites, of which 148 were located in remote settings and 14 in suburban/urban settings. At each site, 25 particles were released every 2 h and tracked back in time for 6 days. Every 2 h, the particles' three-dimensional location, the mixing layer height, the precipitation rate, and the SR were stored.

These airmass histories were then used to solve Eq. (2) for the TC concentrations and Eq. (4) for the source contributions from the different source types. The particles' initial concentrations were set to 0, since modeling simulations showed that on average less than 2% of the initial concentrations for 6-day trajectories arrived at the receptor. The residence time $\Delta t'_{in}$ was set to the trajectory segment time length of 2 h. If the particle was below the mixing layer, the emission rate $\dot{q}_{in}$ was set equal to the 24-h area source normalized by the mixing layer height to convert to volume source, else $\dot{q}_{in}$ was set to 0.

The emissions added to the particle's mixing ratio were from a weighted average of the emission grid cell in which the particle resided and the neighboring cells. The weights were from a two-dimensional Gaussian kernel where the bandwidths were based on the horizontal spread due to turbulent diffusion. This is similar in concept to Gaussian averaging kernels used in forward LPDMs (de Haan, 1999) and allows for fewer particles to be used in the simulation, with the same precision in particle counting statistics. As discussed in the Supplementary information, the counting statistical error in the TC accounted for less than 2% of the total modeling error.

The transmission function p_{in} was calculated by integrating the rate Eqs. (5) and (6) along each particle's trajectory with the rate coefficient parameterized as discussed in Section 2.4.

Specifically, wet deposition was applied to all particles that encountered precipitation, regardless of height, and the washout depth H_w was set to 1000 m. The TC washout ratio was fixed at 10^5 (Eq. (10)), based on the review from Bidleman (1988), and the VOC washout ratio was fixed at 3.5×10^4 (Eq. (11)), the average value estimated from the CAMx model results.

Dry deposition occurred if the particle was below the mixing layer height. The VOC v_d^g was based on the results in Fig. 2 where v_d^g

was a linear interpolation between the January and July equations (Eq. (12)).

$$k_p^w = W_p/H_W \times P = 100 \times P \quad (10)$$

$$k_g^w = W_g/H_w \times P = 35 \times P \quad (11)$$

$$v_d^g = \left(-0.68\,SR^2 + 0.82\,SR + 0.08\right) \times A + \left(-1.34\,SR^2 + 1.93\,SR + 0.1\right) \times (1 - A) \quad (12)$$

where

$A = |(7 - \text{month of year})|/6.$

The v_d^p and VOC transformation rates were made linear functions of SR with free parameters estimated in the optimization process. In this process, the parameters were varied to obtain a best fit to the spatial and seasonal variations in measured TC concentrations and SOC to OC and isoprene SOC to total SOC fractions. The TC concentrations constrained the sum of the primary and secondary TC and the SOC fractions constrained the split between primary and secondary TC and isoprene SOC from other SOCs.

The TC concentrations were from the 148 rural IMPROVE sites measured in 2008. The SOC fractions came from two field studies, one at a suburban site in Research Triangle Park (RTP), North Carolina (Kleindienst et al., 2007), and the second at a rural site in Bondville, Illinois (Lewandowski et al., 2008). At each site, measured SOC marker species were used in a chemical mass balance model to estimate the contributions from biogenic and anthropogenic sources to OC and the SOC fractions for 2- or 3-month periods.

The values used in the optimization process are presented in Table 3. These values have large, poorly quantified uncertainties (Kleindienst et al., 2007) and were not collected in 2008, and the suburban locations may not be representative of the rural IMPROVE sites. Therefore, these values were used as guides as opposed to strict target values in the tuning process.

A manual optimization process was used in which the VOC transformation rates were varied to reproduce the SOC fractions in Table 3, and v_d^p was varied to produce a best fit between simulated and measured TC concentrations. A number of spatial and seasonal metrics were examined, but the primary metrics were the minimization of the bias and maximization of the correlation coefficient in the average seasonal cycle and spatial patterns in the rural 2008 IMPROVE data as shown in Figs. 3 and 4, respectively.

The best-fit v_d^p, Eq. (13), was lower than the average v_d^p from the CASTNET data (Fig. 1) but within the network's site to site variation. Equation (14) presents the best-fit transformation rate coefficient for the highly reactive VOC species (k_{HY}^t). The transformation rates for isoprene (k_{ISOP}^t) and low-yield VOCs (k_{LY}^t) were set to 1/4 and 1/7 of the highly reactive VOCs, respectively.

Table 3
Relative contributions of total SOC and isoprene-derived SOC (Isop-SOC) to OC and SOC from vegetation (Veg-SOC) at Research Triangle Park, NC (RTP) (Kleindienst et al., 2007), and Bondville, IL (Lewandowski et al., 2008), for a summer and winter period.

		SOC/OC	Veg-SOC/OC	Isop-SOC/Veg-SOC
RTP, NC	Summer: Jul–Aug 2003	0.7	0.6	0.45
	Winter: Jan–Feb 2003	0.2	0.15	0.03
Bondville, IL	Summer: Jun–Aug 2004	0.7	0.6	0.6
	Winter: Dec, 2004–Feb 2005	0.3	0.2	0.07

$$v_d^p = 0.022 + 0.17\,SR \quad (13)$$

$$k_{HY}^t = 0.00032 + 0.0032\,SR \quad (14)$$

To test the sensitivity of the simulation to the final set of rate coefficients, each coefficient was independently doubled and the remaining coefficients varied to fit the optimization data. It was found that doubling one rate equation could be compensated for by changes in other rate equations, reproducing the fit to the measured data and the average source apportionment results. For example, doubling v_d^g and increasing k_{HY}^t by 50% resulted in average source attribution results within one percentage point of the final model and similar model performance statistics. This illustrates the ill-conditioned nature of this problem and the fact that additional monitoring data constraints are needed to obtain unique coefficients. It also illustrates that the average source apportionment results are relatively insensitive to the final set of coefficients.

3. Results

3.1. Model optimization period

The results of the model optimization are presented in Figs. 3–5. As shown in Fig. 3, the model reproduces the average seasonal variation of the measured TC concentrations across the United States, with a correlation coefficient of 0.91 and a regression slope of 0.91 between the two aggregated time series. The contributions from the modeled eight source types are also presented in Fig. 3. It is evident that different sources contributed to different seasons. During the summer months, the average TC is predominantly due to biomass burning and SOC from vegetation. Smaller contributions from area and mobile sources also occur. During the winter, vegetation and fire have smaller contributions and area sources are the largest contributor, accounting for about half of the TC. The different fire seasons are also evident, with large contributions during the summer months due to the large wildfires that occur and smaller contributions during the spring and fall when smaller prescribed and agricultural fires tend to occur (Knapp et al., 2009).

As shown in Fig. 4, the simulation reproduces the major features of the annual average TC spatial patterns, with the high TC concentrations along the West Coast and eastern United States and the lower concentrations in the intermountainous West and Great Plains. The average TC concentrations along the West Coast and in the eastern United States had variations of a factor of 2 or more from one site to another. In general, the simulated TC reproduced this variability. Exceptions to the good correspondence occurred in southern California and Mount Baldy, Arizona. At Mount Baldy, the simulation underestimated the measured concentrations by a factor of 3. This bias was primarily due to TC concentrations on September 18 and October 3, when the measured concentrations were 106 μg m^{-3} and 65 μg m^{-3}, respectively, compared to simulated concentrations of 0.8 μg m^{-3} and 0.7 μg m^{-3}, respectively. TC concentration of this magnitude in rural Arizona only occurs due to direct impacts from fire plumes. Elevated TC was not measured at neighboring sites, so the high Mount Baldy TC was most likely due to a smaller fire, such as a prescribed fire, near the monitoring site. Either these fires were missing from the emission inventory or the fire's plume was not properly transported to the receptor site.

In southern California, the measured TC concentrations were overestimated by a factor of 3. The cause of this large overestimation is not known, but this is a particularly challenging region to model, with complex terrain and meteorology and a diverse set of sources. Examination of the source contributions

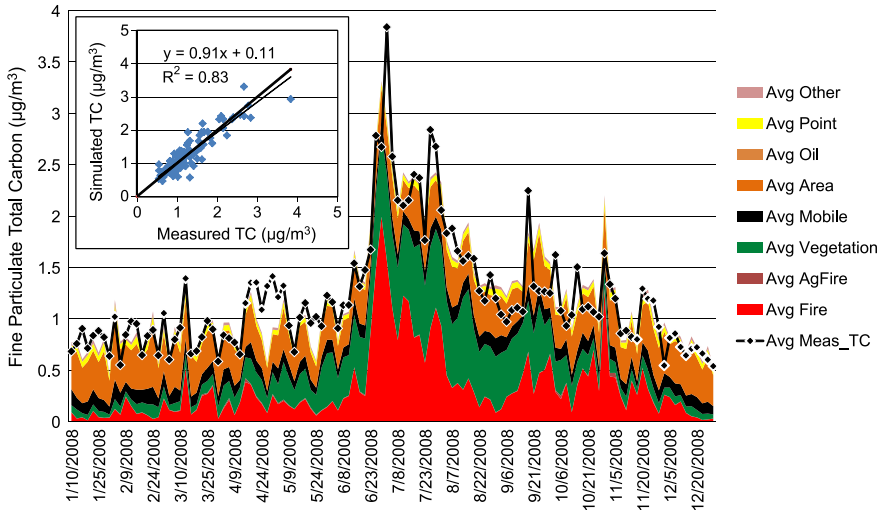

Fig. 3. Comparison of the simulated and measured TC at the IMPROVE monitoring sites during 2008. For each sampling day, the TC concentrations were averaged across all sites.

showed the mobile and area sources together were almost twice the measured TC. Therefore, contributions from these two source sectors were significantly overestimated. The 24-h average emissions used in the model simulations could contribute to this overestimation. However, such an overestimation was not evident in other regions including the east coast, where contributions of area and mobile sources were also relatively high.

The transformation rate coefficients were optimized to approximately reproduce the winter and summer SOC/POC, veg-SOC/POC, and ISOP-SOC/Veg-SOC tracer-derived ratios shown in Table 3. Fig. 5 compares the simulated results to these literature values in scatter plots with the regression line fitted through zero. In this figure, the simulated OC concentrations were estimated by scaling the simulated TC by the average measured OC/TC of 0.8. As shown, there is good correspondence between the measured and simulated SOC fractions, with $r^2 > 0.6$ and slope of the regression line near 1, indicating that on average the simulation reproduced the SOC fractions throughout the year. These results, in conjunction with the good correspondence when simulating the total TC concentrations, indicate that at least in the eastern United States, the model is reproducing the seasonal dynamics in the primary and secondary particulate carbon. Due to the lack of measured SOC tracer concentrations in the western United States, the primary and secondary carbon split cannot be assessed.

3.2. 2006–2008 IMPROVE TC simulation

The optimized CMC model was used to simulate the TC concentrations at the IMPROVE monitoring sites for 2006 and 2007. For each year standard model performance statistics were calculated for each monitoring site. These results are summarized in Table 4, which presents the median and 16th and 84th percentiles of these statistics across the sites by year. Three measurements of error are presented: the relative root mean square error (RMSE), median of the absolute relative error (MdAE) (Hyndman and Koehler, 2006), and fractional error (FE) (Seigneur et al., 2000). The RMSE is the most sensitive to outliers, while the MdAE is least sensitive.

The 2008 simulation had the best overall performance statistics, while 2006 had the lowest, and the performance during 2007 was similar to 2008. All three years had low biases, with typical fractional biases (FB) <0.10 and median correlation between measured

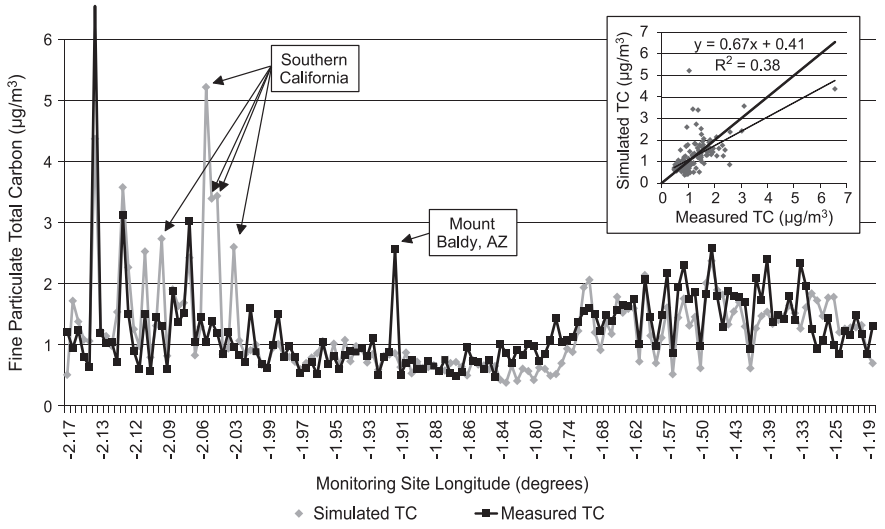

Fig. 4. Comparison of the simulated and measured annual average 2008 TC concentrations at each IMPROVE site. In the line chart, the monitoring sites are sorted from west to east.

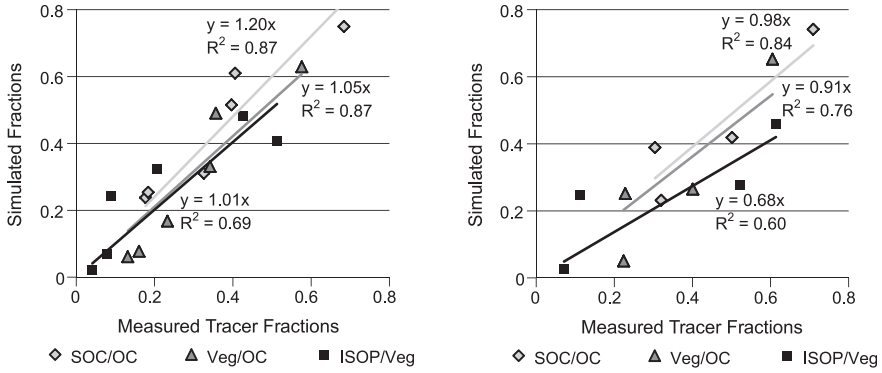

Fig. 5. Simulated fractions of SOC from the CMC model compared to the measured tracer concentrations at RTP, NC (left), and Bondville, IL (right). The November and December tracer-derived SOC data at RTP exclude one outlying sample.

and simulated TC at each monitoring site about 0.57 during 2007 and 2008 and 0.48 in 2006. These correlation coefficients were influenced by outlier data, illustrated by the fact that the typical MdAE was <50% during 2006–2008, but the RMSE was >90% in 2006 and 2007. As demonstrated by the 2008 Mount Baldy simulation (Fig. 3), fires could significantly impact the concentrations. Errors in either the fire emission inventory or meteorology inadvertently transporting smoke to or away from the receptor caused many outlying data points. This could also be intensified by the relatively coarse grid used in the simulation, which artificially spreads out the smoke in the grid cell in which the fire occurs and impacts any receptors within this grid cell.

To help identify spatial variations in the model performance, contour maps of the correlation coefficients, FE, and FB were generated for each simulated year. Fig. 6 presents the results for 2007–2008, and the 2006 results are presented in Fig. S1. The best model performance occurred in the eastern United States, where the correlations for most sites were near 0.7 and above and FE generally <0.5. In the West, the correlations decreased to between 0.5 and 0.7, except in the Northwest and Southwest, where the correlations were often below 0.5. The FE in the West also increased to 0.5 and above, with the highest errors (FE > 0.8) occurring at a number of sites in the coastal states. The high error in southern California was evident in all three years of simulations.

There is systematic spatial variation in the FB where the measured TC in the eastern United States is generally underestimated, but it is overestimated in the western United States. The East also has a north-south gradient, with biases generally between −0.15 and −0.30 in the north and −0.15 to 0.15 in the south. The high errors at the sites in the West Coast states are caused by large FB, often >0.6. Many of the overestimated values had large contributions from nearby fires greater than the measured TC, indicating their contribution to the TC was overestimated.

CMAQ model simulation of 2006 IMPROVE TC data was made available for this study (Pierce, 2010). As discussed in the supplementary information, the CMC model results compared favorably with the CMAQ model performance statistics as well as to past modeling studies. This is evident in Table 4, which shows that the CMAQ simulation generally had better precision but higher bias than the CMC model, resulting in similar total errors.

4. Discussion

The approach for simulating the TC was based on an optimization process such that the simulated TC reproduced the average measured spatial and temporal concentration patterns. A benefit of this process is that the model results could provide sophisticated interpolation and extrapolation of the concentration data in space and time. The model optimization also allowed for the examination of important processes in simulating TC. As expected, it was found that having the correct location and the timing of emissions significantly improved the model's precision. Consequently, a year-specific biomass burning emission inventory was needed as opposed to using a climatological inventory. In addition, the incorporation of precipitation removal significantly improved model precision. On the other hand, variation of the dry deposition and SOC formation rates, whether constant or solar-radiation-dependent, had little influence on the model precision but controlled the relative fractions of primary and secondary TC and the overall model bias.

An important drawback in the optimization process is that the final model compensates for systematic biases in the modeling system used in the optimization, and the model may not be suitable for use at locations and years not used in the optimization process. Another drawback of the approach is that it was based on first-order rate processes to simulate nonlinear chemistry. These

Table 4
Model performance statistics for TC concentration simulations at 148 rural IMPROVE monitoring sites using the CMC model for 2006–2008 and the CMAQ model for 2006.

	2008	2007	2006	CMAQ-2006
Average measured TC, μg m^{-3}	1.04 (0.70, 1.73)	1.10 (0.77, 2.01)	1.14 (0.74, 1.93)	1.14 (0.74, 1.93)
Average simulated TC, μg m^{-3}	1.01 (0.63, 1.71)	1.17 (0.70, 2.04)	1.32 (0.75, 1.95)	1.07 (0.50, 1.74)
Correlation coefficient	0.59 (0.46, 0.71)	0.57 (0.38, 0.72)	0.48 (0.34, 0.64)	0.58 (0.41, 0.73)
Bias of annual means (%)	−2 (−29, 31)	−4 (−25, 33)	6 (−21, 46)	−24 (−42, 19)
Fraction bias	−0.05 (−0.33, 0.30)	−0.08 (−0.32, 0.24)	0.02 (−0.30, 0.35)	−0.36 (−0.59, 0.03)
Fractional error	0.55 (0.42, 0.73)	0.53 (0.44, 0.69)	0.58 (0.44, 0.76)	0.61 (0.48, 0.78)
Relative root mean square error (%)	82 (54, 1.38)	92 (61, 191)	93 (64, 193)	80 (59, 216)
Median of the absolute relative error (%)	45 (33, 60)	45 (34, 57)	48 (36, 70)	46 (39, 57)

For each model performance statistic, the median value across all monitoring sites is presented. The parenthetical values are the 16th and 84th percentiles across the monitoring sites.

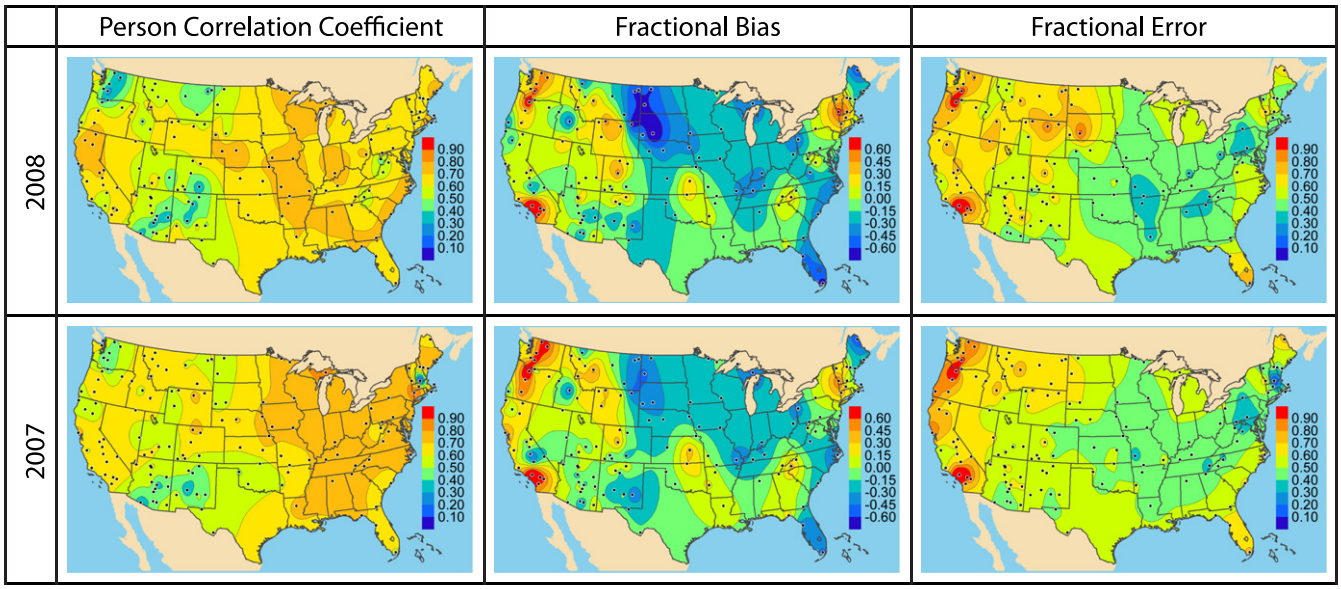

Fig. 6. The 2007 and 2008 CMC model performance statistics from the comparison of simulated to measured TC at rural IMPROVE monitoring sites. The maps were created by first calculating the model performance at each rural IMPROVE site (black dots) then spatially interpolating these data using a Kriging algorithm.

errors may not be significant for simulating the ambient TC concentrations but could adversely affect the relative contributions of the source regions and source types, a sought-after result of the model.

The CMC model generally had good correspondence, with the measured data being able to reproduce the seasonal and spatial variability in the TC concentrations, and its performance is in line with past modeling studies using Eulerian grid models. However, some issues were found. First, the simulated TC at southern California monitoring sites was a factor of 3 larger than measured concentrations, indicating that the model has limited applicability in this region. The IMPROVE network had nine urban sites operating in 2008 and their TC was simulated using the CMC model. Measured TC at these sites was generally underestimated, particularly during the winter months. These sites are more highly influenced by local emissions than the rural sites. The simple dispersion mechanism and coarse meteorological fields used are likely not sufficient to capture the transport dynamics needed for these urban areas. Last, there were similar spatial patterns in the biases and errors in all three simulated years. This indicates that the errors are not the result of anomalous meteorological conditions but instead likely due to errors in the formulation of the model or emission inventory.

Future developments of the model will seek to reduce these errors reflected in the spatial patterns. This will include examining the incorporation of varying land surface types in the dry deposition coefficients. In addition, we will explore the effects of incorporating diurnal cycles in the emission inventory as opposed to using 24-h averages. Last, a formal, statistically robust optimization method will be sought.

These issues in the current model illustrate limitations in such a simple formulation for predictive assessments. The best use of this model is as a low resource and efficient diagnostic tool to provide insights into the sources contributing to TC at remote receptor sites. This would be valuable in weight of evidence source apportionment assessments, such as those conducted to understand the causes of haze at Big Bend, Texas (Schichtel et al., 2005b). This model could also be exercised to guide more resource-intensive analyses, including the operation of Eulerian CTMs. Last, the model was able to reproduce the spatial and temporal measured TC patterns; secondary and primary TC split in the eastern United States; and the CMAQ simulated biomass burning TC (see Supplementary information). It was also found that the average source attribution was relatively insensitive to the set of optimized rate coefficients. Provided outlying concentrations and monitoring sites can be accounted for, the results can be used for climatological analyses of source contributions to the measured TC at receptor sites.

An additional intent in developing this model is to exercise it routinely and to provide its output for IMPROVE monitoring site locations and sample days, available from the IMPROVE website (http://vista.cira.colostate.edu/IMPROVE/). This is done as a service to IMPROVE data users and to aid in the development of Regional Haze State Implementation Plans (Regional Haze Regulations, 1999).

Acknowledgments

We greatly appreciate the contributions of Tom E. Pierce, Chief of the Emissions and Model Evaluation Branch in EPA's Atmospheric Modeling and Analysis Division, who provided the CMAQ model simulation results, and Christine Wiedinmyer, scientist at the National Center for Atmospheric Research, who provided the fire emissions inventory.

This work was supported by the Joint Fire Science Program (09-1-03-1) and the National Park Service (contract #H2370094000). The assumptions, findings, conclusions, judgments, and views presented herein are those of the authors and should not be interpreted as representing the NPS, U.S. EPA, or NOAA policies.

Appendix A. Supplementary information

Supplementary information related to this article can be found online at http://dx.doi.org/10.1016/j.atmosenv.2012.07.017.

References

Andronache, C., 2004. Estimates of sulfate aerosol wet scavenging coefficient for locations in the Eastern United States. Atmospheric Environment 38, 795–804.
Ashbaugh, L.L., 1983. A statistical trajectory technique for determining air pollution source regions. Journal of the Air Pollution Control Association 33, 1096–1098.

Barrie, L.A., 1981. The prediction of rain acidity and SO_2 scavenging in eastern North America. Atmospheric Environment 15, 31–41.
Bidleman, T.F., 1988. Atmospheric processes: wet and dry deposition of organic compounds are controlled by their vapor-particle partitioning. Environmental Science & Technology 22 (4), 361–367.
Black, T.L., 1994. The new NMC mesoscale Eta model: description and forecast examples. Weather Forecasting 9, 265–278.
Bond, T.C., Streets, D.G., Yarber, K.F., Nelson, S.M., Woo, J.-H., Klimont, Z., 2004. A technology-based global inventory of black and organic carbon emissions from combustion. Journal of Geophysical Research 109, D14203. http://dx.doi.org/10.1029/2003JD003697.
Brewer, P., Moore, T., 2009. Source contributions to visibility impairment in the southeastern and western United States. Journal of the Air & Waste Management Association 59, 1070–1081.
Carlton, A.G., Wiedinmyer, C., Kroll, J.H., 2009. A review of secondary organic aerosol (SOA) formation from isoprene. Atmospheric Chemistry & Physics 9, 4987–5005.
de Haan, P., 1999. On the use of density kernels for concentration estimates within particle and puff dispersion models. Atmospheric Environment 33, 2007–2021.
ENVIRON International Corporation, 2010. CAMx User's Guide, Comprehensive Air Quality Model with Extensions. Version 5.30. ENVIRON, 773 San Marin Drive, Suite 2115, Novato, CA 94998, 415.899.0700, also available at: http://www.camx.com/files/CAMxUsersGuide_v5.30.pdf.
Hallquist, M., Wenger, J.C., Baltensperger, U., Rudich, Y., Simpson, D., Claeys, M., Dommen, J., Donahue, N.M., George, C., Goldstein, A.H., Hamilton, J.F., Herrmann, H., Hoffmann, T., Iinuma, Y., Jang, M., Jenkin, M.E., Jimenez, J.L., Kiendler-Scharr, A., Maenhaut, W., McFiggans, G., Mentel, T.F., Monod, A., Prevot, A.S.H., Seinfeld, J.H., Surratt, J.D., Szmigielski, R., Wildt, J., 2009. The formation, properties and impact of secondary organic aerosol: current and emerging issues. Atmospheric Chemistry & Physics 9, 5155–5236.
Hand, J.L., Schichtel, B.A., Pitchford, M., Malm, W.C., Frank, N.H., 2012. Seasonal composition of remote and urban fine particulate matter in the United States. Journal of Geophysical Research 117, D05209. http://dx.doi.org/10.1029/2011JD017122.
Hart, K.M., Tremp, J., Molnar, E., Giger, W., 1993. The occurrence and the fate of organic pollutants in the atmosphere. Water, Air, and Soil Pollution 68, 91–112.
Hennigan, C.J., Miracolo, M.A., Engelhart, G.J., May, A.A., Presto, A.A., Lee, T., Sullivan, A.P., McMeeking, G.R., Coe, H., Wold, C.E., Hao, W.M., Gilman, J.B., Kuster, W.C., de Gouw, J., Schichtel, B.A., Collett Jr., J.L., Kreidenweis, S.M., Robinson, A.L., 2011. Chemical and physical transformations of organic aerosol from the photo-oxidation of open biomass burning emissions in an environmental chamber. Atmospheric Chemistry & Physics Discussion 11, 11995–12037.
Hyndman, R.J., Koehler, A.B., 2006. Another look at measures of forecast accuracy. International Journal of Forecasting 22, 679–688.
Kleindienst, T.E., Jaoui, M., Lewandowski, M., Offenberg, J.H., Lewis, C.W., Bhave, P.V., Edney, E.O., 2007. Estimates of the contributions of biogenic and anthropogenic hydrocarbons to secondary organic aerosol at a southeastern US location. Atmospheric Environment 41, 8288–8300.
Knapp, E.E., Estes, B.L., Skinner, C.N., 2009. Ecological Effects of Prescribed Fire Season: a Literature Review and Synthesis for Managers. General Technical Report PSW-GTR-224. Department of Agriculture, Forest Service, Pacific Southwest Research Station, Albany, California, 80 pp.
Lewandowski, M., Jaoui, M., Offenberg, J.H., Kleindienst, T.E., Edney, E.O., Sheesley, R.J., Schauer, J.J., 2008. Primary and secondary contributions to ambient PM2.5 in the Midwestern United States. Environmental Science & Technology 42, 3303–3309.
Meyers, T.P., Finkelstein, P.L., Clarke, J., Ellestad, T.G., Sims, P.F., 1998. A multilayer model for inferring dry deposition using standard meteorological measurements. Journal of Geophysical Research-Atmospheres 103, 22645–22661.
Ng, N.L., Kwan, A.J., Surratt, J.D., Chan, A.W.H., Chhabra, P.S., Sorooshian, A., Pye, H.O.T., Crounsel, J.D., Wennberg, P.O., Flagan, R.C., Seinfeld, J.H., 2008. Secondary organic aerosol (SOA) formation from reaction of isoprene with nitrate radicals (NO_3). Atmospheric Chemistry & Physics Discussion 8, 3163–3226.
Pierce, T.E., 2010. Personal Communication.
Rodriguez, M.A., Barna, M.G., Gebhart, K.A., Hand, J.L., Adelman, Z.E., Schichtel, B.A., Collett Jr., J.L., Malm, W.C., 2011. Modeling the fate of atmospheric reduced nitrogen during the Rocky Mountain Atmospheric Nitrogen and Sulfur Study (RoMANS): performance evaluation and diagnosis using integrated processes rate analysis. Atmospheric Environment 45, 223–234.
Schichtel, B.A., Husar, R.B., 1997. Regional simulation of atmospheric pollutants with the CAPITA Monte Carlo model. Journal of the Air & Waste Management Association 47, 331–343.
Schichtel, B.A., Barna, M.G., Gebhart, K.A., Malm, W.C., 2005a. Evaluation of an Eulerian and Lagrangian air quality model using perfluorocarbon tracers released in Texas for the BRAVO haze study. Atmospheric Environment 39, 7044–7062.
Schichtel, B.A., Gebhart, K.A., Malm, W.C., Barna, M.G., 2005b. Reconciliation and interpretation of Big Bend National Park particulate sulfur source apportionment: results from the Big Bend regional aerosol and visibility observational study – part I. Journal of the Air & Waste Management Association 55 (11), 1709–1725.
Seibert, P., Frank, A., 2004. Source-receptor matrix calculation with a Lagrangian particle dispersion model in backward mode. Atmospheric Chemistry & Physics 4, 51–63.
Seigneur, C., Pun, B., Pai, P., Louis, J.F., Solomon, P., Emery, C., Morris, R., Zahniser, M., Worsnop, D., Koutrakis, P., White, W., Tombach, I., 2000. Guidance for the performance evaluation of three-dimensional air quality modeling systems for particulate matter and visibility. Journal of the Air & Waste Management Association 50, 588–599.
Stohl, A., 1998. Computation, accuracy and applications of trajectories – a review and bibliography. Atmospheric Environment 32 (6), 947–966.
Uliasz, M., Pielke, R.A., 1992. Receptor-oriented Lagrangian–Eulerian model of mesoscale air pollution dispersion. In: Zannetti, P. (Ed.), Computer Techniques in Environmental Studies, Comput. Mech., Billerica, Mass., pp. 57–68.
Vong, R.J., Vong, I.J., Vickers, D., Covert, D.S., 2010. Size-dependent aerosol deposition velocities during BEARPEX'07. Atmospheric Chemistry and Physics Discussion 10, 4649–4672.
Wiedinmyer, C., Quayle, B., Geron, C., Belote, A., McKenzie, D., Zhang, X., O'Neill, S., Wynne, K.K., 2006. Estimating emissions from fires in North America for air quality modeling. Atmospheric Environment 40 (19), 3419–3432.
Zhang, Y., Huang, J.P., Henze, D.K., Seinfeld, J.H., 2007. Role of isoprene in secondary organic aerosol formation on a regional scale. Journal of Geophysical Research 112, D20207. http://dx.doi.org/10.1029/2007JD008675.